Inhomogeneous phases in the quark-meson model with vacuum fluctuations

Stefano Carignano,[1] Michael Buballa,[2] and Bernd-Jochen Schaefer[3]

[1] *Department of Physics, The University of Texas at El Paso, USA*
[2] *Theoriezentrum, Institut für Kernphysik, Technische Universität Darmstadt, Germany*
[3] *Institut für Theoretische Physik, Justus-Liebig-Universität Gießen, Germany*

Inhomogeneous chiral-symmetry breaking phases at non-vanishing chemical potential and temperature are studied within a two-flavor quark-meson model in the chiral limit. The analysis is performed beyond the standard mean-field approximation by taking into account the Dirac-sea contributions of the quarks. Compared with the case where the Dirac sea is neglected, we find that the inhomogeneous phase shrinks, but in general does not disappear. It is shown within a Ginzburg-Landau analysis that the Lifshitz point of the inhomogeneous phase coincides with the tricritical point if the ratio between sigma-meson and constituent quark mass in vacuum is chosen to be $m_\sigma/M = 2$, corresponding to the fixed mass ratio in the Nambu–Jona-Lasinio model. In the present model, however, this ratio can be varied, offering the possibility to separate the two points. This is confirmed by our numerical calculations, which demonstrate a strong sensitivity of the size of the inhomogeneous phase on m_σ. Finally, we uncover a general instability of the model with respect to large wave numbers of the chiral modulations, which calls for further improvements beyond the present approximation.

arXiv:1404.0057v2 [hep-ph] 9 Jul 2014

I. INTRODUCTION

In spite of the very intensive theoretical and experimental efforts over the past decades, the phase diagram of Quantum Chromodynamics (QCD) is still poorly understood [1, 2]. Most of our current understanding of the QCD phase structure revolves around vanishing quark chemical potential, where ab-initio lattice simulations are reliable [3–6]. In the regime of non-vanishing chemical potential (or net-baryon density), on the other hand, many fundamental questions are still left unanswered, most notably on the nature of the chiral phase transition at low temperatures and the existence of a critical endpoint, for a review see for example [7].

In the past few years, a growing number of indications has been found that strong-interaction matter at high densities might form spatially inhomogeneous phases. This would lead to a dramatic revision of our picture of finite-density QCD. In particular, it has been proposed that the conjectured critical endpoint (CP) of the first-order chiral phase transition might be replaced by a so-called Lifshitz point (LP), where two homogeneous phases and an inhomogeneous phase meet [8].

The concept of spatially dependent order parameters is rather common in condensed matter physics, such as the FFLO state in superconductivity [9, 10] or spin density waves [11], including magnetism [12]. It has been discussed for color superconductivity [13, 14] and for nuclear matter in the context of pion condensation [15], Skyrme crystals [16], and recently in an extended linear sigma model with vector and axial vector mesons [17]. Inhomogeneous chiral-symmetry breaking phases in quark matter have been proposed already long time ago [18–21] but received enhanced attention during the last few years [22–28].

Most of the current studies on strong-interaction matter at finite density are performed within QCD-inspired effective models in mean-field approximation. One of the most widely employed examples is the Nambu–Jona-Lasinio (NJL) model, which, in spite of its simple four-fermion interaction, can be used to describe the phenomenon of spontaneous chiral symmetry breaking and its restoration at finite temperature and density [29–32]. The study of inhomogeneous phases in the NJL model has been performed by several authors [20–24, 26, 28], all with the conclusion that the usual first-order chiral phase transition for homogeneous quark-matter at low temperatures and intermediate densities is surrounded by an inhomogeneous "island". The favored shape for the chiral order parameter is typically one with a one-dimensional spatial modulation [26, 33].

A major drawback of the NJL model is its non-renormalizability: in order to obtain meaningful results, the diverging vacuum contribution from the Dirac sea of the quarks to the grand potential has to be regularized. This introduces ambiguities, since the results depend on the choice of the regularization prescription as well as the value of the corresponding cutoff parameter. In particular, model results are not expected to be reliable for temperatures and chemical potentials bigger than the employed ultraviolet cutoff, which is typically chosen in the range between 0.5 and 1 GeV.

A delicate issue arises when one tries to push the NJL model to high densities, in the regime where large-N_c studies predict the formation of crystalline phases [34–36]. It was recently found that beyond the inhomogeneous island a second inhomogeneous phase emerges and seems to persist up to arbitrarily high chemical potentials. Thorough investigations have established that this inhomogeneous "continent" arises from the interplay of the medium and the

vacuum contributions to the thermodynamic potential and might at least partially be caused by the used regularization [19, 24]. Since these findings are not finally clarified, a similar study of inhomogeneous phases within a renormalizable model is desirable.

For this purpose, and in order to get rid of regularization ambiguities in general, we consider a two-flavor chiral quark-meson (QM) model [37, 38], which represents a renormalizable alternative to the NJL model. In the first QM-model studies the vacuum contribution of the quarks to the grand potential has been neglected because it was expected that a proper refit of the model parameters would compensate the omission of the Dirac sea. However, this "no-sea" or "standard mean-field" approximation (sMFA) has been shown to lead to inconsistent thermodynamics, such as a first-order chiral phase transition in the chiral limit for two flavors at vanishing chemical potential [39]. In this context, the importance of the fermionic vacuum fluctuations for the thermodynamics has been emphasized recently in [40–42] and for three flavors in [43–46].

Inhomogeneous phases in the QM model have already been studied in Ref. [22], but again without taking into account the quark vacuum contributions. In the present work, we improve these investigations by going beyond the sMFA and considering a properly renormalized thermodynamic potential. In this way we obtain a deeper understanding of the effect of quantum and thermal fluctuations on the formation of inhomogeneous phases in QCD matter.

The structure of the paper is as follows: In Sec. II we introduce the model Lagrangian and derive a general expression for the thermodynamic potential, which is the starting point for our later investigations of the phase structure. In Sec. III we restrict our studies to the homogeneous vacuum, focusing on the renormalization of the Dirac-sea contributions. Based on this, we present numerical results for the phase diagram for homogeneous phases in Sec. IV. After that our analysis is extended to include inhomogeneous matter. We begin with a general Ginzburg-Landau analysis in Sec. V, concentrating on the locations of the CP and the LP, and then explore the phase structure for specific one-dimensional modulations in Sec. VI. In Sec. VII our studies are extended to higher chemical potentials, analyzing the existence of a second inhomogeneous phase and its physical nature. Our conclusions are drawn in Sec VIII.

II. THERMODYNAMIC POTENTIAL

The quark-meson model is defined by the Minkowskian Lagrangian density [37, 38, 47, 48]

$$\mathcal{L}_{\mathrm{QM}} = \bar{\psi}\left(i\gamma^\mu\partial_\mu - g(\sigma + i\gamma_5\vec{\tau}\cdot\vec{\pi})\right)\psi + \mathcal{L}_{\mathrm{M}}^{\mathrm{kin}} - U(\sigma,\vec{\pi}) \ , \tag{1}$$

where ψ is a $4N_fN_c$-dimensional quark spinor with $N_f = 2$ flavor and $N_c = 3$ color degrees of freedom, σ is the scalar field of the sigma meson and $\vec{\pi}$ the pseudo-scalar fields of the pion triplet. The meson kinetic contributions reads

$$\mathcal{L}_{\mathrm{M}}^{\mathrm{kin}} = \frac{1}{2}\left(\partial_\mu\sigma\partial^\mu\sigma + \partial_\mu\vec{\pi}\partial^\mu\vec{\pi}\right) \ , \tag{2}$$

while

$$U(\sigma,\vec{\pi}) = \frac{\lambda}{4}\left(\sigma^2 + \vec{\pi}^2 - v^2\right)^2 \tag{3}$$

is an $O(4)$-symmetric meson potential. The $O(4)$-symmetry, which is isomorphic to the chiral $SU(2)_L \times SU(2)_R$ symmetry, can be broken explicitly by adding a term, which is linear in the σ field. However, in this work we will restrict ourselves to the chiral limit and omit such a term. The three model parameters, g, λ and v^2, will be fitted to vacuum properties as discussed in the next section.

The thermodynamic properties of the model are encoded in the grand potential per volume V,

$$\Omega(T,\mu) = -\frac{T}{V}\log\mathcal{Z}(T,\mu) = -\frac{T}{V}\log\int\mathcal{D}\bar{\psi}\mathcal{D}\psi\mathcal{D}\sigma\mathcal{D}\vec{\pi}\exp\left(\int_{V_4} d^4x_E\left(\mathcal{L}_{\mathrm{QM}} + \mu\bar{\psi}\gamma^0\psi\right)\right) \ , \tag{4}$$

where $\mathcal{Z}(T,\mu)$ denotes the grand canonical partition function, which depends on the temperature T and the quark chemical potential μ. The integral in the exponent is performed in Euclidean space-time, $x_E = (\tau,\mathbf{x})$ with the imaginary time $\tau = it$, and extends over the four-volume $V_4 = [0,\frac{1}{T}]\times V$.

Since the Lagrangian is bilinear in the quark fields, the integration over the quarks can be performed analytically. In mean-field approximation we treat the meson fields σ and π^a as classical and replace them by their expectation values [37, 38]. Thereby we also assume these mean fields to be time independent but, in order to allow for inhomogeneous phases, we retain their dependence on the spatial coordinate $\mathbf{x}$. The thermodynamic potential then takes the form

$$\Omega_{\mathrm{MFA}}(T,\mu;\sigma,\vec{\pi}) = -\frac{T}{V}\mathbf{Tr}\,\mathrm{Log}\left(\frac{1}{T}\left(i\partial_0 - H_{\mathrm{QM}} + \mu\right)\right) + \frac{1}{V}\int_V d^3x\,\mathcal{H}_{\mathrm{M}} \ , \tag{5}$$

where the functional trace runs over V_4 and internal (color, flavor and Dirac) degrees of freedom.[1] The mesonic Hamiltonian density and the effective Dirac Hamiltonian are given by

$$\mathcal{H}_{\rm M} = \frac{1}{2}\left((\vec{\nabla}\sigma(\mathbf{x}))^2 + (\vec{\nabla}\vec{\pi}(\mathbf{x}))^2\right) + U(\sigma(\mathbf{x}),\vec{\pi}(\mathbf{x})) \tag{6}$$

and

$$H_{\rm QM} = -i\gamma^0\gamma^i\partial_i + \gamma^0\left(g\sigma(\mathbf{x}) + ig\gamma^5\vec{\tau}\cdot\vec{\pi}(\mathbf{x})\right)\,, \tag{7}$$

respectively. The latter is hermitean, so that, at least in principle, it can be diagonalized. Moreover, since $H_{\rm QM}$ is time-independent, the integration over Euclidean time can be performed in the usual way by summing fermionic Matsubara frequencies. One obtains

$$-\frac{T}{V}\mathbf{Tr}\,\mathrm{Log}\left(\frac{1}{T}\left(i\partial_0 - H_{\rm QM} + \mu\right)\right) = -\frac{1}{V}\sum_\lambda\left[\frac{E_\lambda-\mu}{2} + T\ln\left(1+e^{-\frac{E_\lambda-\mu}{T}}\right)\right]\,, \tag{8}$$

where λ labels the eigenstates of $H_{\rm QM}$ and E_λ are the corresponding eigenvalues. Introducing the density of states

$$\rho(E;\sigma,\vec{\pi}) = \frac{1}{V}\sum_\lambda\delta(E-E_\lambda(\sigma,\vec{\pi})) \tag{9}$$

and exploiting the fact that in all cases which are of interest to us the eigenvalues come in pairs with opposite sign, the thermodynamic potential becomes

$$\Omega_{\rm MFA}(T,\mu;\sigma,\vec{\pi}) = -\int_0^\infty dE\,\rho(E;\sigma,\vec{\pi})\Big\{E + T\log\left[1+e^{-\frac{E-\mu}{T}}\right] + T\log\left[1+e^{-\frac{E+\mu}{T}}\right]\Big\} + \frac{1}{V}\int_V d^3x\,\mathcal{H}_{\rm M}\,. \tag{10}$$

If the meson fields are homogeneous, i.e., if $\sigma(\mathbf{x})$ and $\vec{\pi}(\mathbf{x})$ are constant in space, the quark energies can be labelled by their conserved three-momenta $\mathbf{p}$,

$$E_{\mathbf{p}} = \sqrt{\mathbf{p}^2 + g^2(\sigma^2+\vec{\pi}^{\,2})}\,. \tag{11}$$

The thermodynamic potential then takes the familiar form

$$\Omega_{\rm hom}(T,\mu;\sigma,\vec{\pi}) = -2N_fN_c\int\frac{d^3p}{(2\pi)^3}\left\{E_{\mathbf{p}} + T\log\left[1+e^{-\frac{E_{\mathbf{p}}-\mu}{T}}\right] + T\log\left[1+e^{-\frac{E_{\mathbf{p}}+\mu}{T}}\right]\right\} + \frac{\lambda}{4}\left(\sigma^2+\vec{\pi}^{\,2}-v^2\right)^2\,, \tag{12}$$

which corresponds to the density of states

$$\rho_{\rm hom}(E;\sigma,\vec{\pi}) = \frac{N_fN_c}{\pi^2}E\sqrt{E^2-g^2(\sigma^2+\vec{\pi}^{\,2})}\,\theta\big(E^2-g^2(\sigma^2+\vec{\pi}^{\,2})\big)\,. \tag{13}$$

For non-uniform meson fields, on the other hand, the quark three-momentum is not conserved and the diagonalization of $H_{\rm QM}$ is in general very difficult. Therefore, in this paper, we restrict ourselves to certain one-dimensional spatial modulations for which analytical solutions of the eigenvalue problem exist. This will be discussed in Sec. VI.

III. VACUUM PROPERTIES

In this section we discuss the vacuum properties of the model in order to fix its parameters. In particular, we focus on the renormalization of the quark Dirac sea.

We assume that the vacuum is homogeneous. For the moment, this is simply based on phenomenology, but we will see later that the investigated inhomogeneous solutions are indeed disfavored in vacuum. The thermodynamic potential is then given by the $T=\mu=0$-limit of Eq. (12),

$$\Omega_{\rm vac}(\sigma,\vec{\pi}) = -2N_fN_c\int\frac{d^3p}{(2\pi)^3}\sqrt{\mathbf{p}^2+g^2(\sigma^2+\vec{\pi}^{\,2})} + \frac{\lambda}{4}\left(\sigma^2+\vec{\pi}^{\,2}-v^2\right)^2\,, \tag{14}$$

---

[1] We will always refer to $\Omega_{\rm MFA}$ for any given σ and $\vec{\pi}$ as "thermodynamic potential" even though strictly speaking this term should only be used for the function evaluated at the physical minimum.

where we have inserted the quark energies Eq. (11). Minimization with respect to the sigma and pion mean fields, $\partial\Omega_{\rm vac}/\partial\sigma = \partial\Omega_{\rm vac}/\partial\pi^a = 0$, and assuming that the pion fields vanish, the nontrivial solution for the sigma field satisfies the gap equation

$$\lambda\left(\sigma^2 - v^2\right) = 2N_f N_c\, g^2 \int \frac{d^3p}{(2\pi)^3}\, \frac{1}{\sqrt{\mathbf{p}^2 + g^2\sigma^2}}\,. \tag{15}$$

In the following we will denote the solution of this equation by $\langle\sigma\rangle$. From the Lagrangian we can then identify the constituent quark mass as

$$M \equiv g\langle\sigma\rangle\ . \tag{16}$$

For later convenience we also define the corresponding quark propagator in Minkowski space,

$$S_F(p) = \frac{1}{\not{p} - M + i\epsilon}\,, \tag{17}$$

and the loop integral

$$L_1 = 4iN_fN_c \int \frac{d^4p}{(2\pi)^4}\, \frac{1}{p^2 - M^2 + i\epsilon} = 2N_fN_c \int \frac{d^3p}{(2\pi)^3}\, \frac{1}{\sqrt{\mathbf{p}^2 + M^2}}\ , \tag{18}$$

which allows to write the gap equation as

$$\lambda\left(\frac{M^2}{g^2} - v^2\right) = g^2\, L_1\,. \tag{19}$$

A. Standard mean-field approximation

The thermodynamic potential as well as the momentum integral L_1 are divergent and one has to specify how to treat them in order to obtain well-defined results. The integral is related to the Dirac sea of the quarks and it was a standard procedure for a long time to neglect this divergent vacuum contribution to the potential completely ("no-sea" or "standard mean-field" approximation, sMFA) [38]. The vacuum thermodynamic potential is then entirely given by the mesonic potential,

$$\Omega_{\rm vac}^{\rm sMFA}(\sigma,\vec{\pi}) \equiv U(\sigma,\vec{\pi}) = \frac{\lambda}{4}\left(\sigma^2 + \vec{\pi}^{\,2} - v^2\right)^2\ , \tag{20}$$

and the gap equation (19) simplifies to

$$\frac{M^2}{g^2} - v^2 = 0\,. \tag{21}$$

We determine the three model parameters, g, λ and v^2 by fitting the pion decay constant f_π, the constituent quark mass M and the sigma meson mass to fixed values. f_π is related to M and the quark-pion coupling constant g_π by the Goldberger-Treiman relation,

$$M = g_\pi f_\pi\,. \tag{22}$$

In sMFA the coupling g_π is equal to the bare Yukawa coupling g, which is therefore given by

$$g = \frac{M}{f_\pi}. \tag{23}$$

Inserting this into the gap equation (21) yields

$$v^2 = f_\pi^2\ . \tag{24}$$

From Eqs. (16) and (23) one also finds $\langle\sigma\rangle = f_\pi$, i.e., f_π corresponds to the vacuum expectation value of the sigma field. As we will see below, this does no longer hold when one goes beyond sMFA.

The meson masses in sMFA are given by the curvature of the thermodynamic potential at the physical minimum. Since $\Omega_{\rm vac}^{\rm sMFA}$ is equal to the meson potential U, see Eq. (20), this is equal to the so-called tree-level masses, given by

$$m_{j,t}^2 = \left.\frac{\partial^2 U}{\partial \phi_j^2}\right|_{\sigma=\langle\sigma\rangle,\vec{\pi}=0} , \tag{25}$$

where $\phi_j \in \{\sigma, \vec{\pi}\}$. For the sigma meson one obtains

$$m_{\sigma,t}^2 = \lambda\left(3\langle\sigma\rangle^2 - v^2\right) = 2\lambda f_\pi^2 , \tag{26}$$

where we employed the identities $\langle\sigma\rangle = v = f_\pi$ derived above. This fixes the quartic coupling constant as

$$\lambda = \frac{m_\sigma^2}{2f_\pi^2} . \tag{27}$$

The pion mass vanishes,

$$m_{\pi,t}^2 = \lambda\left(\langle\sigma\rangle^2 - v^2\right) = 0 , \tag{28}$$

in consistency with the Goldstone theorem.

B. Including the Dirac sea

We now add the Dirac-sea contribution to the thermodynamic potential. In this way certain quantum fluctuations which are neglected in the sMFA are taken into account. Since the additional term affects the vacuum properties of the model, a refit of the parameters becomes necessary. We thereby assume that the divergent momentum integrals are regularized in some way, so that the expressions can be manipulated in a mathematically well-defined manner. Details of the used regularization are irrelevant at this stage and will be postponed to Sec. III C where the numerical evaluations will be discussed.

The constituent quark mass is given by the gap equation (19), now including the Dirac-sea contribution L_1, which depends on M as well. We can use this equation to express the parameter v^2 in terms of M and the other two parameters g and λ,

$$v^2 = \frac{M^2}{g^2} - \frac{g^2 L_1}{\lambda} . \tag{29}$$

For the determination of the meson masses and f_π further preparations are needed. As in the sMFA, the tree-level masses $m_{j,t}$ are defined via the second derivatives of the meson potential U at the minimum of the thermodynamic potential, Eq. (25). However, due to the Dirac sea, the minimum of $\Omega_{\rm vac}$ does no longer coincide with the minimum of U. As a consequence, despite the same definition, the results are shifted by $g^2\, L_1$:

$$\begin{aligned} m_{\sigma,t}^2 &= g^2\, L_1 + 2\lambda\langle\sigma\rangle^2 , \\ m_{\pi,t}^2 &= g^2\, L_1 . \end{aligned} \tag{30}$$

In particular, the tree-level pion gets massive, and we have to include loop-corrections in order to restore the Goldstone theorem. To this end we define the tree-level propagators in the meson channel $j \in \{\sigma, \vec{\pi}\}$

$$iD_{j,t}(q^2) = \frac{i}{q^2 - m_{j,t}^2 + i\epsilon} , \tag{31}$$

and dress them with quark-antiquark polarizations loops,

$$-i\Pi_j(q^2) = -\int \frac{d^4p}{(2\pi)^4} \mathrm{tr}\left[\Gamma_j iS_F(p+q)\Gamma_j iS_F(p)\right] , \tag{32}$$

where $\Gamma_\sigma = \mathbb{1}$ and $\Gamma_{\pi^a} = i\gamma_5\tau^a$. Summing up a geometrical series of these self-energy insertions, as diagrammatically

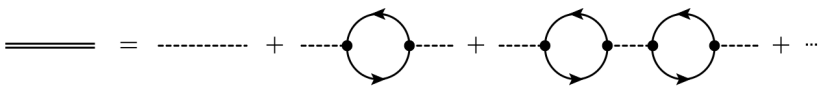

FIG. 1. Resummation of quark-antiquark polarization loops. The bare meson propagators are indicated by dashed lines, the dressed meson propagator by the double line. The filled circles indicate the bare Yukawa coupling g.

depicted in Fig. 1, we obtain the dressed meson propagator

$$D_j(q^2) = \frac{1}{q^2 - m_{j,t}^2 + g^2\Pi_j(q^2) + i\epsilon} \,. \tag{33}$$

The pole mass m_j is defined by the implicit equation

$$D_j^{-1}(q^2 = m_j^2) \stackrel{!}{=} 0 \,, \tag{34}$$

and we expand

$$\Pi_j(q^2) = \Pi_j(m_j^2) + \Pi'(m_j^2)(q^2 - m_j^2) + \dots \,, \tag{35}$$

with $\Pi' \equiv \frac{d}{dq^2}\Pi(q^2)$. The propagator in the vicinity of the pole is then given by

$$D_j(q^2) = \frac{Z_j}{q^2 - m_j^2 + i\epsilon} \;+\; \text{regular terms} \,, \tag{36}$$

with the wave-function renormalization constant

$$Z_j = \frac{1}{1 + g^2\Pi_j'(m_j^2)} \,. \tag{37}$$

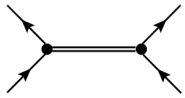

FIG. 2. Exchange of a dressed meson between quarks.

Hence, if the meson is exchanged between two quarks, as depicted in Fig. 2, we encounter the combination

$$g^2 D_j(q^2) \equiv \frac{g_j^2}{q^2 - m_j^2 + i\epsilon} \,, \tag{38}$$

which allows us to identify the renormalized quark-meson coupling constant at the pole as[2]

$$g_j = g\sqrt{Z_j} \,. \tag{39}$$

The explicit evaluation of the polarization loops for the sigma and pion channel is rather standard and has been presented, e.g., in the context of mesonic excitations in the NJL model [30], where exactly the same integrals appear. One finds

$$\begin{aligned} \Pi_\pi(q^2) &= L_1 - \frac{1}{2}q^2 L_2(q^2) \,, \\ \Pi_\sigma(q^2) &= L_1 - \frac{1}{2}(q^2 - 4M^2) L_2(q^2) \,, \end{aligned} \tag{40}$$

[2] Alternatively, this result also follows in a straightforward way from the Lagrangian by introducing a wave-function renormalization for the mesons while leaving the quark fields unrenormalized.

with the loop integrals L_1, defined in Eq. (18), and

$$L_2(q^2) = 4iN_fN_c \int \frac{d^4p}{(2\pi)^4} \frac{1}{[(p+q)^2 - M^2 + i\epsilon][p^2 - M^2 + i\epsilon]}$$
$$= 4N_fN_c \int \frac{d^3p}{(2\pi)^3} \frac{1}{\sqrt{\mathbf{p}^2 + M^2}} \frac{1}{q^2 - 4(\mathbf{p}^2 + M^2) + i\epsilon} \,. \tag{41}$$

Inserting this together with the the tree-level masses, Eq. (30), into Eq. (33), we obtain the dressed meson propagators

$$D_\pi(q^2) = \frac{1}{q^2\left(1 - \frac{1}{2}g^2 L_2(q^2)\right)} \,, \tag{42}$$

$$D_\sigma(q^2) = \frac{1}{q^2 - \frac{1}{2}g^2(q^2 - 4M^2)L_2(q^2) - 2\lambda M^2/g^2} \,, \tag{43}$$

where in the second equation we have employed Eq. (16) to express the sigma field through the constituent quark mass.

The first equation immediately shows that the pion propagator has a pole at $q^2 = 0$, i.e.,

$$m_\pi = 0 \,, \tag{44}$$

which is consistent with the Goldstone theorem. For the wave-function renormalization constant at the pole we read off

$$Z_\pi = \frac{1}{1 - \frac{1}{2}g^2 L_2(0)} \,, \tag{45}$$

which yields the renormalized quark-pion coupling constant

$$g_\pi^2 = \frac{g^2}{1 - \frac{1}{2}g^2 L_2(0)} \,. \tag{46}$$

Hence, employing the Goldberger-Treiman relation Eq. (22), the pion decay constant is given by

$$f_\pi^2 = \frac{M^2}{g^2}\left(1 - \frac{1}{2}g^2 L_2(0)\right) \,, \tag{47}$$

which can be used to fix the Yukawa coupling g:

$$g^2 = \frac{M^2}{f_\pi^2 + \frac{1}{2}M^2 L_2(0)} \,. \tag{48}$$

For the pole mass of the sigma meson, Eq. (43) yields the relation

$$m_\sigma^2 - \frac{1}{2}g^2(m_\sigma^2 - 4M^2)L_2(m_\sigma^2) - 2\lambda\frac{M^2}{g^2} = 0 \,, \tag{49}$$

which can be used to fix the quartic coupling constant:

$$\lambda = 2g^2\frac{m_\sigma^2}{4M^2}\left[1 - \frac{1}{2}g^2\left(1 - \frac{4M^2}{m_\sigma^2}\right)L_2(m_\sigma^2)\right] \,. \tag{50}$$

In the NJL model the sigma-meson mass in the chiral limit is always equal to $2M$ [30]. In the QM model there is no such restriction, but for $m_\sigma = 2M$ the expression for λ becomes particularly simple: The L_2-term drops out, and we find $\lambda = 2g^2$.

For arbitrary sigma masses it is useful to separate

$$L_2(m_\sigma^2) = L_2(0) + \delta L_2(m_\sigma^2) \,, \tag{51}$$

where $\delta L_2(m_\sigma^2)$ is a finite expression. We can then employ Eq. (47) to express $L_2(0)$ through f_π and get

$$\lambda = 2g^2\left[1 + g^2\left(\frac{m_\sigma^2}{4M^2} - 1\right)\left(\frac{f_\pi^2}{M^2} - \frac{1}{2}\delta L_2(m_\sigma^2)\right)\right] \,. \tag{52}$$

Finally, we briefly comment on the so-called screening masses of the mesons which are defined in analogy to the tree-level masses, Eq. (25), but with the meson potential U replaced by the thermodynamic potential Ω, i.e., in vacuum,

$$m_{j,s}^2 = \left.\frac{\partial^2 \Omega_{\rm vac}}{\partial \phi_j^2}\right|_{\sigma=\langle\sigma\rangle,\vec{\pi}=0} . \tag{53}$$

These masses are related to the unrenormalized dressed meson propagator for vanishing momentum, $D_j(0) = -1/m_{j,s}^2$, so that $m_{\pi,s} = 0$, in agreement with the pole mass. For the sigma meson, on the other hand, one finds

$$m_{\sigma,s}^2 = 2\lambda\frac{M^2}{g^2} - 4M^2 + 4g^2 f_\pi^2 = \frac{g^2 f_\pi^2}{M^2} m_\sigma^2 + (4M^2 - m_\sigma^2)\frac{1}{2} g^2 \delta L_2(m_\sigma^2) \,, \tag{54}$$

which coincides with the pole mass in the sMFA, but is different when the quark loops are taken into account. Hence, fixing the screening mass of the sigma rather than the pole mass, as was done, e.g., in Ref. ,[39], leads in general to a different value for λ. However, we consider the pole mass as the more physical quantity (see also Ref. [49]) and fix λ from Eq. (52).

In summary, the model parameters v^2, g, and λ are determined by the equations (29), (48), and (52), respectively, for fixed values of M, m_σ and f_π, and a given regularization procedure to tame the loop integrals L_1 and L_2. This program will be discussed next in detail.

C. Regularization and parameter fixing

For the regularization of the quark loops, we employ the Pauli-Villars (PV)-inspired scheme developed in Ref. [22]. In this scheme, the divergent term in the general expression for the mean-field thermodynamic potential, Eq. (10), is replaced in the following way:

$$-\int_0^\infty dE\, \rho(E;\sigma,\vec{\pi})\, E \;\to\; -\int_0^\infty dE\, \rho(E;\sigma,\vec{\pi}) \sum_{j=0}^{3} c_j \sqrt{E^2 + j\Lambda^2} \,, \tag{55}$$

with a cutoff parameter Λ and the coefficients $c_0 = 1$, $c_1 = -3$, $c_2 = 3$, and $c_3 = -1$. In homogeneous matter, following the same steps as before, this amounts to the standard PV regularization,

$$\int \frac{d^3p}{(2\pi)^3}\, F(M^2) \;\to\; \int \frac{d^3p}{(2\pi)^3} \sum_{j=0}^{3} c_j\, F(M^2 + j\Lambda^2) \tag{56}$$

of the loop integrals L_1 and $L_2(q^2)$. Explicitly, one finds

$$L_1 \to \frac{N_f N_c}{4\pi^2} \sum_{j=0}^{3} c_j M_j^2 \ln M_j^2 \,, \tag{57}$$

$$L_2(0) \to \frac{N_f N_c}{4\pi^2} \sum_{j=0}^{3} c_j \ln M_j^2 \,, \tag{58}$$

$$\mathrm{Re}\,\delta L_2(q^2) \to \frac{N_f N_c}{4\pi^2} \sum_{j=0}^{3} c_j \left\{ f\left(\frac{4M_j^2}{q^2} - 1\right) - 2 \right\}, \tag{59}$$

$$\mathrm{Im}\,\delta L_2(q^2) \to -\frac{N_f N_c}{4\pi} \sum_{j=0}^{3} c_j \sqrt{1 - \frac{4M_j^2}{q^2}}\, \theta(q^2 - 4M^2) \,, \tag{60}$$

with $M_j^2 = M^2 + j\Lambda^2$ and

$$f(x) = \begin{cases} 2\sqrt{x}\arctan(\frac{1}{\sqrt{x}}) \,, & x > 0 \\ \sqrt{-x}\ln(\frac{1+\sqrt{-x}}{1-\sqrt{-x}}) \,, & x < 0 \\ 0 \,, & x = 0 \,. \end{cases} \tag{61}$$

Similar to Eq. (51), we have split the function $L_2(q^2)$ into two parts, $L_2(0)$ and $\delta L_2(q^2)$. Since the latter is finite, its regularization is not necessary. We prefer, however, to regularize the entire function $L_2(q^2)$. This has the advantage that the sMFA results are recovered when the limit $\Lambda \to 0$ is taken. For $\Lambda \to \infty$, on the other hand, the regularization of $\delta L_2(q^2)$ makes no difference, as the regulator terms, corresponding to $j = 1, 2, 3$, vanish, and only the $j = 0$ term survives.

We also note that δL_2 receives an imaginary part above the two-quark threshold, $q^2 > 4M^2$. This becomes relevant for $m_\sigma > 2M$ and signals a non-vanishing width of the sigma meson due to quark-antiquark decay. In the parameter fit we will then define the sigma mass as the point where the real part of the inverse sigma propagator vanishes.

As an alternative to the PV prescription, we could regularize the divergencies with a sharp three-momentum cutoff. For homogeneous phases both schemes give similar results, as will be shown in Sec. IV. We note, however, that a momentum cutoff is not appropriate for inhomogeneous phases. Intuitively this can be seen from the fact that a restriction of the individual quark momenta would also restrict the possible wave numbers of the inhomogeneity. A more formal argument will be given in Sec. V in the context of a Ginzburg-Landau analysis.

Throughout this paper, we fix the vacuum values of the constituent quark mass to $M = 300$ MeV and of the pion decay constant to its chiral-limit value $f_\pi = 88$ MeV. For the sigma-meson mass we will take the NJL-model relation $m_\sigma = 2M = 600$ MeV . Later, in Sec. VI B, m_σ will be varied in order to study its influence on the phase diagram.

Numerical results for the parameters as functions of the cutoff in the PV regularization scheme are shown in Fig. 3. For a sharp $O(3)$ cutoff the behavior is qualitatively similar. At a certain value of Λ, the couplings g^2 and λ diverge and change their sign. As can be seen from Eqs. (48) and (50), this happens at the point where $f_\pi^2 = -\frac{1}{2}M^2 L_2(0)$. Interestingly, this is exactly the expression for f_π^2 in the NJL model [30]. The parameter v^2 changes its sign as well, although at a different value of Λ. Above this point the chiral-symmetry breaking is no longer caused by the meson potential, like in the sMFA, but by the Dirac sea of the quarks. As one can see from Eqs. (48) and (52) the coupling constants g^2 and λ approach zero when the cutoff goes to infinity. It follows from Eq. (54) that the screening mass of the sigma meson vanishes as well in this limit, whereas the pole mass stays constant by construction. Moreover, since $\mathrm{Im}\,\delta L_2(q^2)$ stays finite while g^2 goes to zero, the decay width of the sigma meson into two quarks also vanishes, even for $m_\sigma > 2M$.

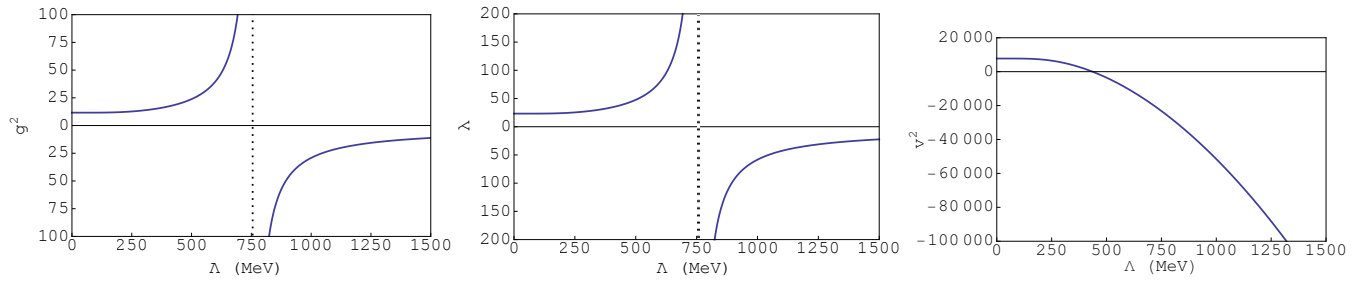

FIG. 3. The model parameters g^2, λ and v^2 (left to right) as functions of the PV cutoff parameter.

IV. NUMERICAL RESULTS FOR HOMOGENEOUS PHASES

We now extend the calculations to nonvanishing temperature and chemical potential. As a first step, and in order to set the stage for our subsequent studies of inhomogeneous phases, we restrict ourselves to homogeneous order parameters. To this end, the thermodynamic potential, Eq. (12), is minimized, now including the T- and μ-dependent terms. Since these terms are convergent, we leave them unregularized (as customary in the sMFA) and only regularize the vacuum term in the way discussed in the previous section.

Numerical results for the phase diagram are presented in Fig. 4. The various solid and dashed lines indicate the phase boundaries obtained with Pauli-Villars regularization and three-momentum cutoff, respectively, using different values of Λ. The dotted line corresponds to the sMFA result. It is well known that in the chiral limit and without the Dirac sea contribution, the Quark-Meson model exhibits a first-order transition along the entire phase boundary, i.e., even at vanishing chemical potential [38, 50]. This problem was carefully analyzed in Ref. [39], where it was identified as an artifact of the sMFA, which is cured when the Dirac-sea contributions are included. Indeed, for both regularization schemes we find that already for $\Lambda = 300$ MeV there is a tricritical point (CP), which separates the first-order transition at higher μ from a second-order one at low μ, both for PV regularization and for a three-momentum cutoff. When Λ is increased further, the second-order part of the transition line continues to grow, so that the CP moves to higher chemical potentials. This can be interpreted as the effect of the vacuum fluctuations, which smoothen

the transition [39]. The fluctuations also increase the "bag pressure", i.e., the pressure difference between the chirally broken and restored vacuum solutions. As a consequence, the phase boundary is shifted to higher temperatures and chemical potentials.

At the same time, the phase diagrams for the two different regularizations become more and more similar, until beyond $\Lambda \approx 1$ GeV the transition lines and the location of the critical point basically overlap. This is of course the expected behavior for a renormalizable model: with a proper rescaling of the parameters, at high values of Λ the results become cutoff-independent. For practical purposes, in the following we will interpret results calculated at a $\Lambda = 5$ GeV cutoff to be the "renormalized" ones. A numerical cross-check performed at $\Lambda = 10$ GeV confirms the stability of these results.

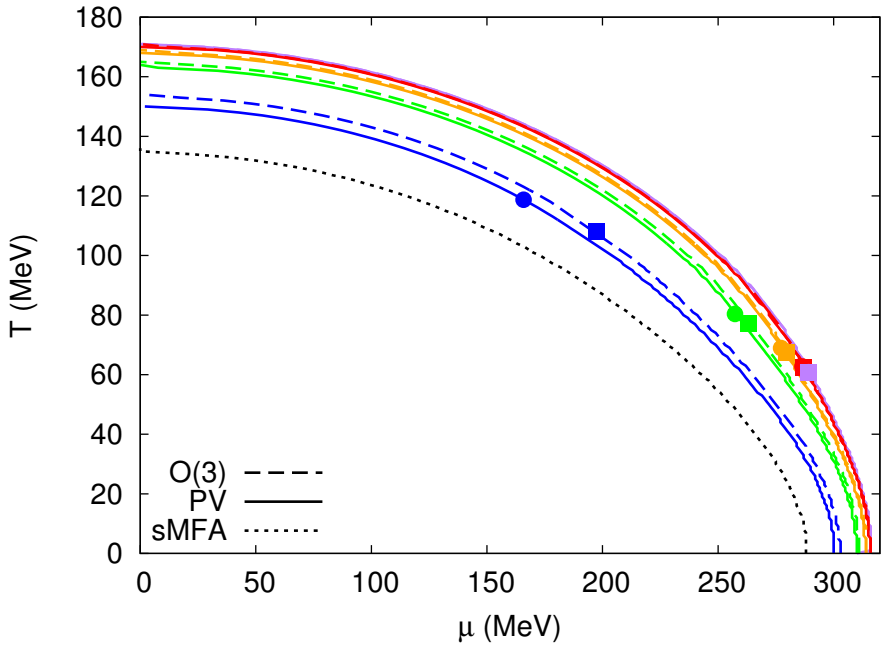

FIG. 4. Phase diagrams for homogeneous condensates. The dotted line indicates the first-order phase boundary in the sMFA. For the other lines the Dirac sea was included, using PV regularization (solid lines) or a sharp three-momentum cutoff (dashed lines), with different values of the cutoff: $\Lambda = 300$ MeV, 600 MeV, 1 GeV, 2 GeV, 5 GeV (from bottom to top). The filled circles (for PV) and squares (for three-momentum cutoff) indicate the tricritical points, separating second-order (to the left) from first-order (to the right) phase transitions.

V. GINZBURG-LANDAU ANALYSIS

Before extending our numerical calculations to investigate inhomogeneous phases, we first want to explore the possible phase structure within a Ginzburg-Landau (GL) approach. In particular we are interested in the Lifshitz point (LP), i.e., the point where the inhomogeneous phase and the two homogeneous phases with broken and restored chiral symmetry meet, and its location relative to the tricritical point (CP), where the second-order chiral phase transition turns into first order if the analysis is restricted to homogeneous phases. Within the GL approach, this can be analyzed in a rather general way, without specifying the explicit form of the inhomogeneity [8, 22, 33].

In the following, we basically extend the analysis of Ref. [22] to include the Dirac sea. For this, the mean-field thermodynamic potential, Eq. (5), is expanded around the symmetric ground state in terms of the order parameters and their gradients. We restrict ourselves to a single isospin component of the pion field, $\pi^a(\mathbf{x}) = \pi(\mathbf{x})\delta_{a3}$, which is sufficient to describe the phases we are interested in. The thermodynamic potential can then be expressed in terms of a complex constituent-quark mass function

$$M(\mathbf{x}) = g\left(\sigma(\mathbf{x}) + i\pi(\mathbf{x})\right) , \tag{62}$$

and the GL expansion takes the form

$$\Omega_{\rm MFA}(T,\mu;M) = \Omega_{\rm MFA}(T,\mu;0) + \frac{1}{V}\int d^3x \left\{ \frac{1}{2}\gamma_2 |M(\mathbf{x})|^2 + \frac{1}{4}\gamma_{4,a}|M(\mathbf{x})|^4 + \frac{1}{4}\gamma_{4,b}|\nabla M(\mathbf{x})|^2 + \dots \right\} . \tag{63}$$

As in Refs. [8, 22], we assume that terms of order 6 or higher are positive. As we will see later, the predictions based on this assumption are confirmed by direct numerical computations of the phase diagram.

In order to compute the GL coefficients γ_i we decompose $\Omega_{\rm MFA}$ into a quark-loop contribution given by

$$\Omega_{q\bar{q}}(T,\mu;M) = -\frac{T}{V}\mathbf{Tr}\,\mathrm{Log}\left(\frac{1}{T}\left(i\partial_0 + H_{\rm QM} - \mu\right)\right), \tag{64}$$

and a pure meson contribution

$$\Omega_{\rm M}(M) = \frac{1}{V}\int_V d^3x\,\mathcal{H}_{\rm M}\,, \tag{65}$$

and expand both parts in the same manner,

$$\Omega_{q\bar{q}}(T,\mu;M) = \Omega_{q\bar{q}}(T,\mu;0) + \frac{1}{V}\int_V d^3x\,\left\{\frac{1}{2}\beta_2|M(\mathbf{x})|^2 + \frac{1}{4}\beta_{4,a}|M(\mathbf{x})|^4 + \frac{1}{4}\beta_{4,b}|\nabla M(\mathbf{x})|^2 + \dots\right\}, \tag{66}$$

$$\Omega_{\rm M}(M) = \Omega_{\rm M}(0) + \frac{1}{V}\int_V d^3x\,\left\{\frac{1}{2}\alpha_2|M(\mathbf{x})|^2 + \frac{1}{4}\alpha_{4,a}|M(\mathbf{x})|^4 + \frac{1}{4}\alpha_{4,b}|\nabla M(\mathbf{x})|^2 + \dots\right\}, \tag{67}$$

so that $\gamma_i = \alpha_i + \beta_i$.

The mesonic coefficients are easily obtained from Eqs. (3) and (6), yielding

$$\alpha_2 = -\frac{\lambda v^2}{g^2}\,, \quad \alpha_{4,a} = \frac{\lambda}{g^4}\,, \quad \alpha_{4,b} = \frac{2}{g^2}\,, \tag{68}$$

while, except for a trivial constant in β_2, the quark-loop terms are the same as in the NJL model [8, 22]. They are given by

$$\beta_2 = \beta_2^{\rm vac} + \beta_2^{\rm med}\,, \tag{69}$$

$$\beta_{4,a} = \beta_{4,b} = \beta_4^{\rm vac} + \beta_4^{\rm med}\,, \tag{70}$$

with the vacuum parts

$$\beta_2^{\rm vac} = -L_1\big|_{M=0}\,, \tag{71}$$

$$\beta_4^{\rm vac} = -L_2(0)\big|_{M=0}\,, \tag{72}$$

and the explicitly T- and μ-dependent medium parts

$$\beta_2^{\rm med} = 2N_fN_c\int\frac{d^3p}{(2\pi)^3}\,\frac{1}{|\mathbf{p}|}\,(n(\mathbf{p}) + \bar{n}(\mathbf{p}))\,, \tag{73}$$

$$\beta_4^{\rm med} = -N_fN_c\int\frac{d^3p}{(2\pi)^3}\,\frac{1}{|\mathbf{p}|^3}\left(n(\mathbf{p}) + \bar{n}(\mathbf{p}) + \frac{|\mathbf{p}|}{T}\Big[n(\mathbf{p})\,(1-n(\mathbf{p})) + \bar{n}(\mathbf{p})\,(1-\bar{n}(\mathbf{p}))\Big]\right), \tag{74}$$

where $n(\mathbf{p}) = 1/[e^{(|\mathbf{p}|-\mu)/T}+1]$ and $\bar{n}(\mathbf{p}) = 1/[e^{(|\mathbf{p}|+\mu)/T}+1]$ are Fermi distribution functions for massless quarks and antiquarks, respectively.

The coefficients $\beta_4^{\rm vac}$ and $\beta_4^{\rm med}$ both exhibit logarithmic divergencies in the infrared, which cancel each other if they are summed. In the sMFA, where the vacuum term is absent, this cancellation does not occur and this originates the artifact that the first-order phase transition extends up to $\mu = 0$ [39]. In addition, the vacuum parts of the β coefficients are ultraviolet divergent, as obvious from the presence of the loop integrals L_1 and L_2. In order to be consistent with our numerical studies of the phase diagram, these integrals are regularized in the same way as described in Sec. III C, while the UV-finite medium parts are left unmodified.

The most important result is that $\beta_{4,a}$ and $\beta_{4,b}$ are equal[3], with the consequence that in the NJL model the LP coincides with the CP [8]. Because of the α-coefficients, this is not necessarily true in the QM model. In general,

[3] The proof of this equality requires an integration by parts and relies on the assumption that there are no surface contributions to the integral. This assumption would be violated by introducing a sharp momentum cutoff, which is our main reason not to use cutoff regularization for inhomogeneous phases.

the CP is given by the condition that the coefficients of the quadratic and quartic terms vanish, while at the LP the quadratic and the gradient terms are zero,

$$\gamma_2\big|_{\rm CP} = \gamma_{4,a}\big|_{\rm CP} = 0\,, \tag{75}$$

$$\gamma_2\big|_{\rm LP} = \gamma_{4,b}\big|_{\rm LP} = 0\,. \tag{76}$$

Since $\beta_{4,a} = \beta_{4,b} \equiv \beta_4$, both conditions are fulfilled simultaneously if $\alpha_{4,a} = \alpha_{4,b}$, i.e., if $\lambda = 2g^2$. As can be seen from Eq. (50), this is the case if $m_\sigma = 2M$, which is just the NJL-model relation between sigma and constituent quark mass in the chiral limit. This result is quite remarkable. It means that if m_σ and M fulfill the NJL-model relation, the LP and the CP coincide, just as they do in the NJL model.[4] We note that we would not have obtained this result if we had determined λ by fitting the screening mass of the sigma meson instead of the pole mass.

In contrast to the NJL model, however, the ratio of m_σ and M can be chosen freely in the QM model, and we thus have the possibility to separate the two points. At the LP, the coefficient $\gamma_{4,a}$, which vanishes at the CP, takes the value

$$\gamma_{4,a}\big|_{\rm LP} = \alpha_{4,a} - \alpha_{4,b} = 2\left(\frac{m_\sigma^2}{4M^2} - 1\right)\left(\frac{f_\pi^2}{M^2} - \frac{1}{2}\delta L_2(m_\sigma^2)\right)\,, \tag{77}$$

where we have used Eq. (52) to eliminate the coupling constants. For m_σ close to $2M$ we can then expand

$$0 = \gamma_{4,a}\big|_{\rm CP} = \gamma_{4,a}\big|_{\rm LP} + \left.\frac{\partial\beta_4}{\partial T}\right|_{\rm LP}\Delta T + \left.\frac{\partial\beta_4}{\partial\mu}\right|_{\rm LP}\Delta\mu\,, \tag{78}$$

where $\Delta T = T_{\rm CP} - T_{\rm LP}$ and $\Delta\mu = \mu_{\rm CP} - \mu_{\rm LP}$ are the temperature and chemical-potential shifts of the CP relative to the LP. At the same time we must require that γ_2 stays zero, i.e.,

$$\left.\frac{\partial\beta_2}{\partial T}\right|_{\rm LP}\Delta T + \left.\frac{\partial\beta_2}{\partial\mu}\right|_{\rm LP}\Delta\mu = 0\,, \tag{79}$$

so that we obtain for the shifts:

$$\Delta T = \left.\left(\frac{\frac{\partial\beta_2}{\partial\mu}}{\frac{\partial\beta_2}{\partial T}\frac{\partial\beta_4}{\partial\mu} - \frac{\partial\beta_2}{\partial\mu}\frac{\partial\beta_4}{\partial T}}\,\gamma_{4,a}\right)\right|_{\rm LP}\,, \tag{80}$$

$$\Delta\mu = \left.\left(\frac{-\frac{\partial\beta_2}{\partial T}}{\frac{\partial\beta_2}{\partial T}\frac{\partial\beta_4}{\partial\mu} - \frac{\partial\beta_2}{\partial\mu}\frac{\partial\beta_4}{\partial T}}\,\gamma_{4,a}\right)\right|_{\rm LP}\,. \tag{81}$$

Hence, even without working out the T and μ derivatives of the β-coefficients, it becomes clear that the sign change of $\gamma_{4,a}|_{\rm LP}$ at $m_\sigma = 2M$ implies that ΔT and $\Delta\mu$ change their signs as well. This strongly suggests that we can realize two different scenarios: one where the CP lies inside the inhomogeneous phase and one where it is outside. We will investigate this numerically in Sect. VI B. Until then, we will concentrate on the NJL-like case $m_\sigma = 2M$.

VI. INHOMOGENEOUS PHASES

We now proceed with the numerical study of the phase diagram, including the possibility of inhomogeneous phases, i.e., allowing the mesonic mean fields to be non-uniform in space. For simplicity, we will restrict ourselves to certain one-dimensional modulations for which analytical expressions for the quark spectral density $\rho(E;\sigma,\vec{\pi})$ are known. In particular, we will focus on the chiral density wave (CDW) ansatz, which amounts to a one-dimensional plane-wave type modulation of the chiral condensate [20–22]. Choosing, as customary, the modulation to point to the z direction, the mesonic mean fields are given by

$$\sigma(z) = \frac{\Delta}{g}\cos(2qz)\,, \qquad \pi(z) = \frac{\Delta}{g}\sin(2qz)\,, \tag{82}$$

[4] For the sMFA, this result is basically contained in the expressions derived in Ref. [22], but was missed due to a simple algebraic mistake.

where the pion field is again restricted to the third isospin component, $\pi^a(z) = \pi(z)\delta_{a3}$. The mean fields can be combined into the complex order parameter

$$M(z) = g(\sigma(z) + i\pi(z)) = \Delta e^{2iqz} \,. \tag{83}$$

Hence, the modulation is characterized by two variational parameters, an amplitude Δ and a wave number q, which can both be chosen to be real and nonnegative. The factor of 2 in the exponent is just to be consistent with current conventions (e.g., [22, 51]). The corresponding quark spectral density reads [22]

$$\begin{aligned}\rho(E;\sigma,\vec{\pi}) = \rho_{\rm CDW}(E;\Delta,q) = N_f N_c \frac{E}{2\pi^2}\Big\{&\theta(E-q-\Delta)\sqrt{(E-q)^2-\Delta^2}\,+\\ &\theta(E-q+\Delta)\,\theta(E+q-\Delta)\sqrt{(E+q)^2-\Delta^2}\,+\\ &\theta(q-\Delta-E)\left(\sqrt{(E+q)^2-\Delta^2}-\sqrt{(E-q)^2-\Delta^2}\right)\Big\}\,,\end{aligned} \tag{84}$$

while for the meson contribution to the thermodynamic potential we have

$$\begin{aligned}\frac{1}{V}\int d^3x\,\mathcal{H}_{\rm M} &= \frac{1}{L}\int_0^L dz\left\{-\frac{1}{2}\left[-\left(\frac{\partial\sigma}{\partial z}\right)^2-\left(\frac{\partial\pi}{\partial z}\right)^2\right]+\frac{\lambda}{4}\left(\sigma^2+\pi^2-v^2\right)^2\right\}\\ &= \frac{1}{2}\left(\frac{2q\Delta}{g}\right)^2+\frac{\lambda}{4}\left[\left(\frac{\Delta}{g}\right)^2-v^2\right]^2\,,\end{aligned} \tag{85}$$

where $L = \pi/q$ is the period of the spatial modulation. Inserting this into Eq. (10), we obtain the thermodynamic potential

$$\Omega_{\rm CDW}(T,\mu;\Delta,q) \equiv \Omega_{\rm MFA}(T,\mu;\sigma,\vec{\pi}) \tag{86}$$

with σ and $\vec{\pi}$ given by Eq. (82). As in the homogeneous case, which is contained in the above expressions as the limit $q \to 0$, we only regularize the vacuum part, now exclusively employing the PV scheme, Eq. (55).

It can be shown on general grounds that for small values of the wave number q the thermodynamic potential at zero temperature and chemical potential rises proportional to $f_\pi^2 q^2$, when expanded around the homogeneous ground state [19]. More precisely, when we define

$$\Delta\Omega_{\rm vac}(q) \equiv \Omega_{\rm CDW}(0,0;M,q) - \Omega_{\rm CDW}(0,0;M,0)\,, \tag{87}$$

with M being the constituent quark mass in vacuum, we expect that

$$\Delta\Omega_{\rm vac}(q) = \frac{1}{2}f_\pi^2(2q)^2 + \mathcal{O}(q^4)\,. \tag{88}$$

In order to show this, we split $\Delta\Omega_{\rm vac}$ into the Dirac-sea contribution of the quarks and the kinetic contribution of the mesons,

$$\Delta\Omega_{\rm vac}(q) = \Delta\Omega_{{\rm vac},q\bar{q}}(q) + \Delta\Omega_{\rm vac,M}(q)\,, \tag{89}$$

with

$$\Delta\Omega_{{\rm vac},q\bar{q}}(q) = -\int_0^\infty dE\Big(\rho_{\rm CDW}(E;M,q) - \rho_{\rm CDW}(E;M,0)\Big)\sum_j c_j\sqrt{E^2+j\Lambda^2} \tag{90}$$

and

$$\Delta\Omega_{\rm vac,M}(q) = \frac{1}{2}\left(\frac{2qM}{g}\right)^2\,. \tag{91}$$

In the sMFA, we have $\Delta\Omega_{{\rm vac},q\bar{q}} = 0$, and Eq. (88) follows immediately from the Goldberger-Treiman relation, Eq. (23). When the Dirac sea is included, one finds

$$\Delta\Omega_{{\rm vac},q\bar{q}}(q) = -M^2 L_2(0) q^2 + \mathcal{O}(q^4)\,, \tag{92}$$

(see appendix) and Eq. (88) is obtained with Eq. (47). This demonstrates that our treatment of inhomogeneous phases is consistent with the parameter fixing in vacuum.

Our numerical results for $\Delta\Omega_{\rm vac}$ are displayed in Fig. 5 against q^2. At low momenta the agreement with $\frac{1}{2}f_\pi^2(2q)^2$ (dashed line) is excellent, while at higher wave numbers the higher-order contributions become visible.

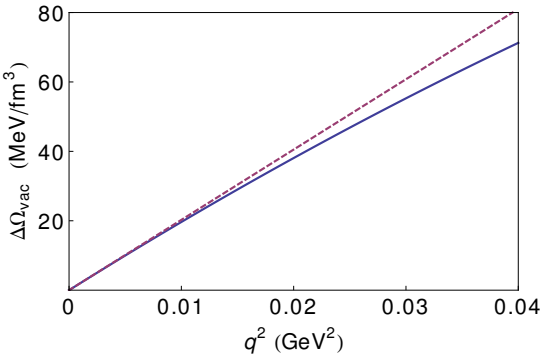

FIG. 5. $\Delta\Omega_{\rm vac}$ as a function of q^2 (solid line), compared with the leading-order behavior $\frac{1}{2}f_\pi^2(2q)^2$ (dashed line). The calculations have been performed with $\Lambda = 5$ GeV.

A. Phase diagram for $m_\sigma = 2M$

Turning on finite temperature and chemical potential and minimizing at each T and μ the thermodynamic potential with respect to Δ and q we obtain the phase diagrams shown in Fig. 6. The three panels correspond to different values of the PV cutoff, $\Lambda = 0$, 600 MeV and 5 GeV. The shaded areas indicate the CDW-type inhomogeneous regions, characterized by nonvanishing values of Δ and q. At the upper-μ side of these regions, the amplitude Δ smoothly goes to zero, corresponding to a second-order phase transition to the restored phase. At the lower-μ side, on the other hand, we find a first-order phase transition, where an inhomogeneous solution with a nonvanishing amplitude and $q > 0$ is degenerate with a homogeneous solution where $q = 0$.

For the sigma-meson mass we have employed the NJL relation $m_\sigma = 2M$. From the GL analysis of Sec. V we expect for this case an inhomogeneous phase ending at a Lifshitz point which coincides with the critical point of the homogeneous calculation. Our numerical results are in perfect agreement with this expectation. In the sMFA, as we have seen in Sec. IV, there is no CP in the homogeneous case. Consequently, when we allow for CDW-type solutions, there is no LP either, and the inhomogeneous phase extends to the T-axis (left panel). A similar result was already obtained in Ref. [22] for a different modulation. However, when the Dirac sea is included (middle and right panels), the inhomogeneous phase shrinks and a Lifshitz point appears, coinciding with the corresponding critical point in Fig. 4. Increasing the cutoff reduces the size of the inhomogeneous phase but does not destroy it, and beyond $\Lambda = 2$ GeV its size stays almost constant. The renormalized QM model in extended mean-field approximation therefore still features an inhomogeneous phase with the same qualitative properties as the NJL model (as long as $m_\sigma = 2M$). In particular, the first-order phase boundary of the homogeneous case is completely covered by the inhomogeneous phase.

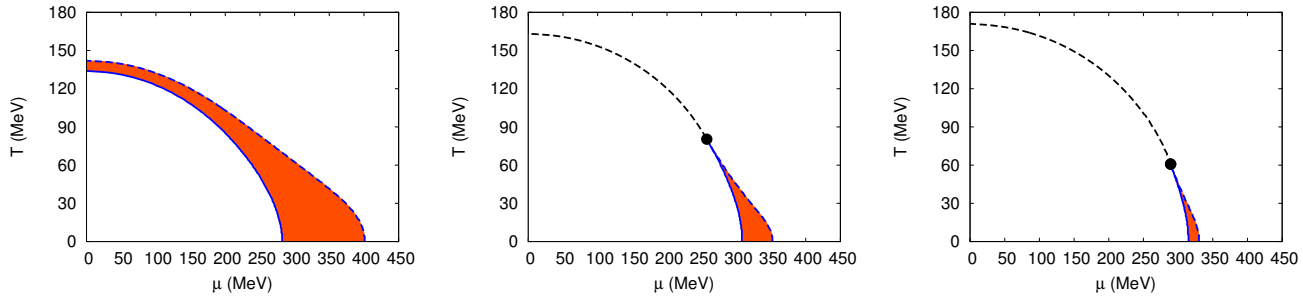

FIG. 6. Phase diagram, allowing for CDW modulations of the order parameter. Left: results obtained in the sMFA. Middle: including the Dirac sea with $\Lambda = 600$ MeV. Right: "renormalized" results obtained with $\Lambda = 5$ GeV. First-order phase transitions are indicated by solid lines, second-order transitions by dashed lines. The shaded areas indicate the inhomogeneous phase, the black dot denotes the Lifshitz point, coinciding with the location of the critical point for homogeneous phases.

In light of previous studies in the NJL model [22–24], we expect the results on the phase structure to be qualitatively independent of the shape of the modulation considered. In fact, as long as the phase transitions are second order, the position of the LP is completely fixed by the GL analysis of Sec. V and therefore independent on the modulation. This argument can be extended to the entire second-order phase boundary from the inhomogeneous to the chirally restored phase. The phase transition from the homogeneous chirally broken to the inhomogeneous phase, on the other

hand, is first order for the CDW and therefore not universal.

For completeness, we therefore briefly consider a different kind of modulation, namely a one-dimensional real soliton lattice of the form [22]

$$M(z) = \Delta\nu \frac{sn(\Delta z, \nu) cn(\Delta z, \nu)}{dn(\Delta z, \nu)}\,, \tag{93}$$

where sn, cn and dn are Jacobi elliptic functions with elliptic modulus $\nu \in [0, 1]$ and a dimensionful parameter Δ. This ansatz, which has been adapted from the $1+1$ dimensional Gross-Neveu model [52] to the $3+1$ dimensional case, corresponds to the most favored inhomogeneous solution known so far, both for the NJL model and for the QM model. It interpolates smoothly between a single domain-wall soliton ($\nu = 1$) and a sinusoidal shape ($\nu = 0$), and allows for second-order phase transitions on both sides, i.e., to the homogeneous broken and restored phases. Since for this kind of modulation the quark spectral density is also known analytically, the formalism is identical to the one employed for the CDW, the only difference being the function $\rho(E; \sigma, \vec{\pi})$ and the spatial average of the mesonic Hamiltonian density in Eq. (85). Details can be found in Ref. [22].

In Fig. 7 we compare the renormalized ($\Lambda = 5$ GeV) phase diagram for the solitonic modulation with the one obtained for the CDW. As expected, and just like in the NJL model, the onset of the inhomogeneous phase slightly moves to lower chemical potential, while the transition to the chirally restored phase and the location of the LP[5] are left unchanged. Except for the order of the phase transition between inhomogeneous and homogeneous broken phase, no new qualitative differences arise.

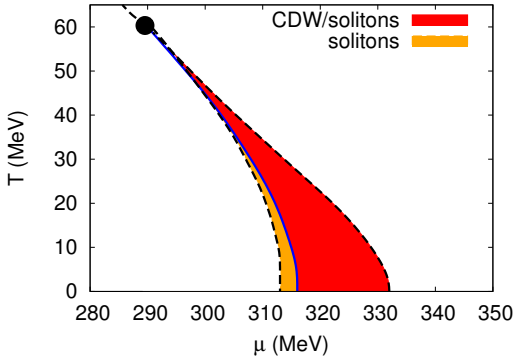

FIG. 7. Comparison of the renormalized ($\Lambda = 5$ GeV) inhomogeneous phase diagrams for the solitons and the CDW modulation. The light shaded area denotes the region where only solitonic solutions are favored over the homogeneous phases. In the dark shaded area the CDW is favored over the homogeneous phases as well, but still disfavored against the solitonic modulation. The dashed lines are second-order phase transitions. The solid line denotes the first-order phase transition at the onset of the CDW phase if solitonic solutions are not considered.

B. Sensitivity of the phase structure on the sigma mass

In this section we want to investigate the sensitivity of the phase structure on the sigma mass. Empirically, the use of different input values for m_σ is justified since the identification of the corresponding resonance, for example $f_0(600)$ [53], is not yet fully established. Indeed, some authors favor a higher mass (above 1 GeV) for the chiral partner of the pion and suggest that the f_0 is a tetraquark or two-meson bound state [54, 55]. A strong sigma-mass sensitivity on the homogeneous phase structure, including the existence of a CP has been observed in various two- and three- flavor quark-meson models with and without the Polyakov-loop [56]. Moreover, as we have seen in Sec. V, the coincidence of the LP and the CP is special to the NJL mass ratio, $m_\sigma/M = 2$. Thus, choosing different ratios offers the possibility to separate the two points.

In the following, various values around $m_\sigma = 600$ MeV are chosen while the constituent quark mass will be kept constant at $M = 300$ MeV in vacuum. In Fig. 8 we show the critical and Lifshitz points, as determined from the

[5] Strictly speaking, a Lifshitz point is a point where three second-order phase boundaries meet. This is the case for the solitonic modulation but not for the CDW. However, since the location of the point is the same, we call it LP in both cases.

GL conditions Eqs. (75) and (76), for different values of the sigma mass. One can see that both points are rather sensitive to a change of m_σ, and the trajectories cross each other at $m_\sigma = 600$ MeV, as expected. However, while both points move to higher chemical potentials when m_σ is increased, the CP is shifted to lower and the LP to higher temperatures. From this behavior we expect that for $m_\sigma > 2M$ the CP is covered by the inhomogeneous phase and thus disappears from the phase diagram. For $m_\sigma < 2M$, on the other hand, the CP is outside of the inhomogeneous region, so that at least a part of the first-order phase boundary between the homogeneous chirally broken and restored phases survives.

In this context we recall that the GL analysis is only reliable for small values of the order parameter and its derivatives. Therefore the prediction for the LP for $m_\sigma < 2M$ becomes questionable, since in this case it could lie inside the spinodal region of the homogeneous first-order phase transition where a homogeneous solution with large mass could be favored.

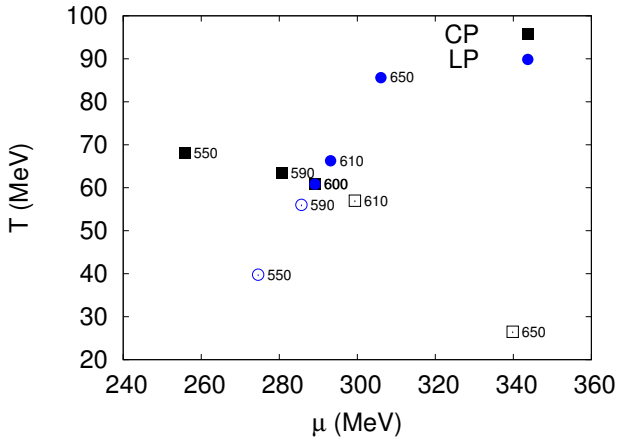

FIG. 8. Location of the critical (black squares) and Lifshitz (blue circles) points according to the Ginzburg-Landau analysis for $\Lambda = 5$ GeV. The numbers indicate the corresponding values of the sigma mass in MeV. The full circles are reliable, the empty ones are not because the analysis is invalidated by the homogeneous first-order phase transition. The critical points indicated by open squares are only relevant if the analysis is restricted to homogeneous phases.

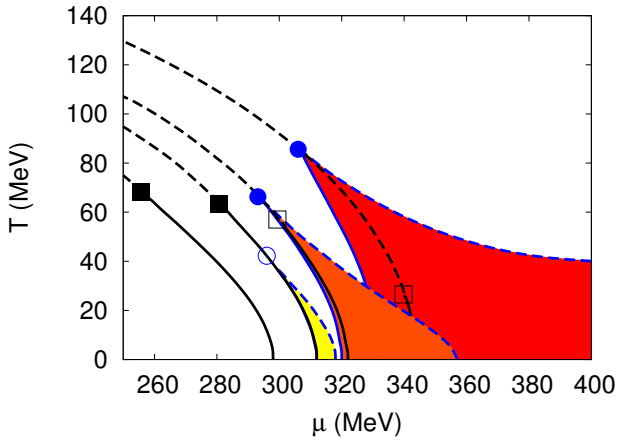

FIG. 9. Phase diagrams for different sigma masses, evaluated with $\Lambda = 5$ GeV. From left to right: $m_\sigma = 550, 590, 610$ and 650 MeV. The shaded areas indicate the regions where the CDW is favored. The black lines denote the phase boundaries between homogeneous phases (solid: first-order; dashed: second-order). Filled squares are the corresponding true CPs, while open squares indicate the locations of the CPs which would be present in a homogeneous analysis but are covered by the inhomogeneous phase. Filled circles are the LPs which agree with the predictions of the GL analysis, while the open circle indicates the point where the inhomogeneous phase ends on the first-order phase boundary between homogeneous phases, and which does not agree with the LP of the GL analysis.

A full numerical study leads to the results displayed in Fig. 9, where we show the phase diagrams obtained for four different values of the sigma mass. For the inhomogeneous phase we restrict ourselves to the CDW ansatz. The

qualitative behavior is in good agreement with our expectations from the GL analysis, but as explained above, there are quantitative deviations for $m_\sigma < 2M$. In this case the inhomogeneous phase shrinks even more quickly with decreasing m_σ than predicted by the GL analysis, and already at $m_\sigma = 570$ MeV it disappears completely. Above this value, but still below $m_\sigma = 600$ MeV, a small inhomogeneous region exists, ending on the first-order phase boundary between the homogeneous phases. For $m_\sigma > 2M$, on the other hand, the size of the inhomogeneous region is strongly enhanced, and the CP lies inside that region.

VII. MODEL ARTIFACTS, ISLANDS AND CONTINENTS

In this section we investigate in more detail the phase structure at higher chemical potentials. Previous studies of inhomogeneous phases within the Nambu–Jona-Lasinio model exhibit the appearance of a second inhomogeneous phase at high densities, which seems to extend up to arbitrarily high chemical potentials [24] . In general, such a behavior is quite common in the literature: Inhomogeneous phases extending to arbitrarily high chemical potentials are also found in lower-dimensional models [51, 52], in large-N_c QCD [34, 35], in particular in the context of quarkyonic matter [36], as well as in Dyson-Schwinger studies of three-color QCD [27] if color-superconductivity effects are neglected. However, in these systems the critical temperature of the inhomogeneous phase typically stays constant or decreases with increasing chemical potential, whereas in the NJL model it grows. Hence, it is unlikely that this inhomogeneous "continent" is a genuine physical feature.

Since the continent appears in a region where the chemical potential is of the order of the NJL-model cutoff, it seems obvious that it is caused by the regularization. On the other hand, the formation of an inhomogeneous phase is known to be a medium-induced effect [20, 21, 36], related to the medium term of the thermodynamic potential, which is typically *not* regularized. It has therefore been argued that the inhomogeneous continent cannot be a trivial regularization artifact, but rather an effect arising from the interplay between the vacuum and the medium contributions in the thermodynamic potential [24]. Of course, caution in the interpretation of model results is always necessary as soon as the chemical potential exceeds the model cutoff. Hence, a similar analysis within the QM model might help to elucidate the physical relevance of the inhomogeneous continent.

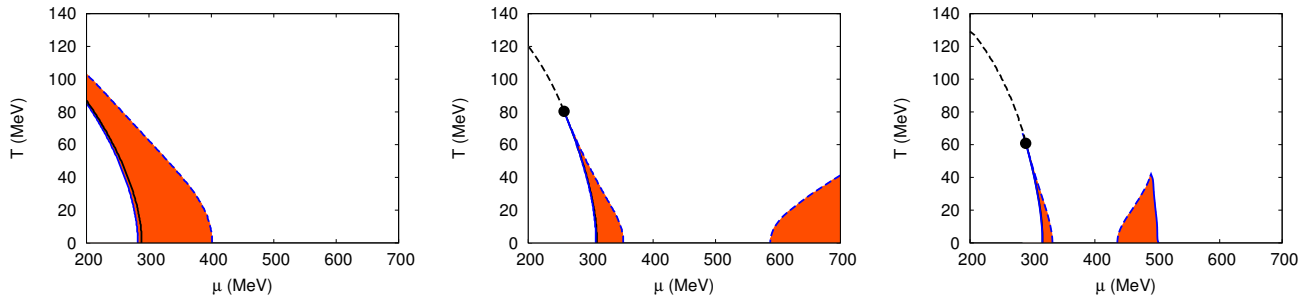

FIG. 10. The same phase diagrams as in Fig. 6, extended to higher chemical potentials (Left: sMFA, middle: $\Lambda = 600$ MeV, right: $\Lambda = 5$ GeV).

For this purpose, we extend the phase diagrams of Fig. 6 to higher μ and investigate the appearance of a second inhomogeneous phase. The results are shown in Fig. 10, again without (left) and with (middle and right) the Dirac-sea contribution. As one can see, the latter has a strong influence on the existence and the properties of the second inhomogeneous phase.

In the left phase diagram, calculated in sMFA, no new inhomogeneous phase appears at high densities. The kinetic term in the meson potential, Eq. (85), disfavors solutions with high q, which are characteristic of the inhomogeneous continent [24]. Including the vacuum contribution, the picture changes significantly. For an intermediate cutoff value of, e.g., $\Lambda = 600$ MeV (middle panel of Fig. 10), a second inhomogeneous region appears and, just like in the NJL model, seems to extend up to arbitrarily high values of the chemical potential.

Again a completely different behavior arises when the Pauli-Villars cutoff is increased beyond the point where the model parameters g^2 and λ diverge and change their sign, i.e., in our case at $\Lambda \approx 750$ MeV (cf. Fig. 3). In this case we still find a second inhomogeneous phase, but restricted to a finite region. This is shown in the right panel of Fig. 10 for $\Lambda = 5$ GeV, where the solution disappears above $\mu \gtrsim 500$ MeV. This disappearance however is not related to a transition to a more favored phase, but rather to an instability. This can be seen from the mesonic contribution to the thermodynamic potential, Eq. (85), which becomes unbounded from below with respect to Δ when λ gets negative and with respect to q when g^2 gets negative. Instabilities with respect to the chiral order parameter have already

been observed for the homogeneous vacuum [39]. This is illustrated in the right panel of Fig. 11, where one can see that the thermodynamic potential is unbounded from below at large values of Δ. For comparison the behavior for a smaller cutoff is shown in the left panel. In both cases, the vacuum constituent mass, which was fixed to 300 MeV by our renormalization procedure (cf. Sec. III C), corresponds to a minimum. However, for $\Lambda = 600$ MeV it is a global minimum, whereas for $\Lambda = 5$ GeV it is only a local one, followed by a maximum beyond which the potential decreases without bounds. One can show that this problem is caused by the one-loop approximation [57], and it can be cured by going beyond the present approximation, e.g., with non-perturbative functional methods such as the functional renormalization group, cf. [50].

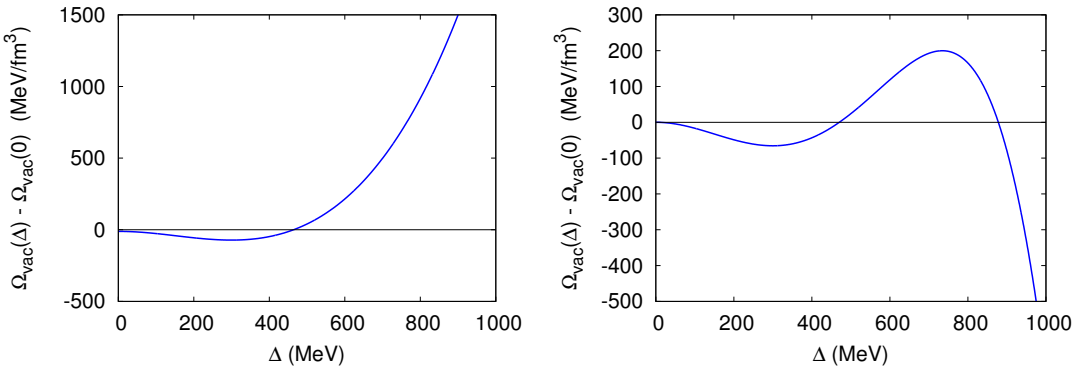

FIG. 11. Thermodynamic potential $\Omega_{\rm vac}(\Delta) \equiv \Omega_{\rm vac}(\sigma = \frac{\Delta}{g}, \vec{\pi} = 0)$ for the homogeneous vacuum relative to the free energy of the chirally restored vacuum, $\Omega_{\rm vac}(0)$, as a function of the order parameter Δ for $\Lambda = 600$ MeV (left) and 5 GeV (right).

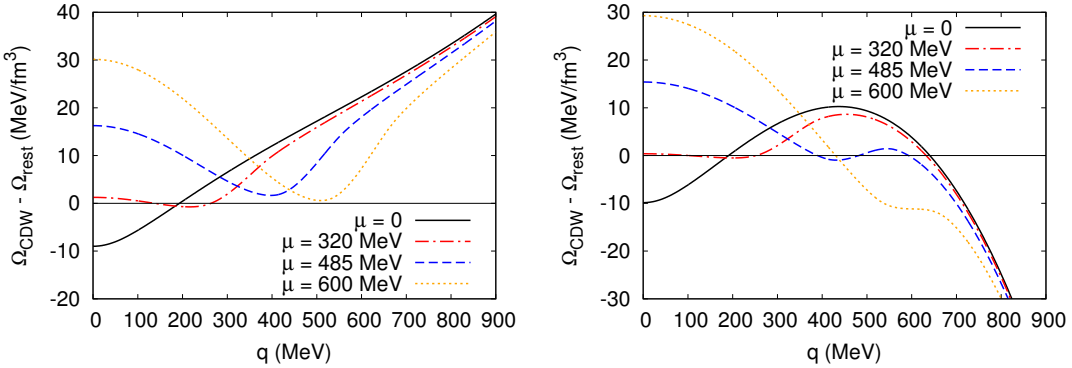

FIG. 12. CDW thermodynamic potential $\Omega_{\rm CDW}(T = 0, \mu; \Delta = 75 \text{ MeV}, q)$ for four different chemical potentials μ, relative to the restored phase $\Omega_{\rm rest} \equiv \Omega_{\rm CDW}(0, \mu; 0, 0)$ as a function of the wave number q for $\Lambda = 600$ MeV (left) and 5 GeV (right).

When CDW modulations are considered, a similar situation arises with respect to the wave number. This is demonstrated in Fig. 12 where the thermodynamic potential for $T = 0$ and four different chemical potentials is plotted as a function of q at a fixed amplitude Δ. For $\Lambda = 600$ MeV (left panel) no instability occurs, whereas for $\Lambda = 5$ GeV (right panel) the thermodynamic potentials are again unbounded from below. In the latter case we observe that already in vacuum (solid line) the homogeneous chirally broken solution at $q = 0$ only corresponds to a local minimum, while arbitrarily large negative values of the thermodynamic potential are reached at large q. Interestingly, a similar behavior was already discussed more than 20 years ago in Ref. [19] for slightly different models.

Comparing the different curves in Fig. 12, one sees that the local minima move towards higher wave numbers with increasing chemical potential. The modifications of the thermodynamic potential are essentially restricted to wave numbers of the order of μ or less (cf. Eqs. (10) and (84)), i.e., they do not affect the behavior at high q. As a consequence, the instabilities for large cutoffs persist. For 5 GeV (right panel), there are still local minima for $\mu = 320$ (dash-dotted line) and 485 MeV (dashed line), which can be related to the first and the second inhomogeneous region in the phase diagram, respectively, (cf. right panel of Fig. 10).[6] Eventually, however, the minimum joins with the

[6] As explained earlier, the phase diagrams are obtained by minimization of $\Omega_{\rm CDW}$ with respect to Δ and q. In order to keep the

maximum and disappears. At $\mu = 600$ MeV (dotted line) there is therefore only an inflection point while the local minimum is gone.

Hence, we failed to clarify the situation at large chemical potentials: While in the NJL model (or in the QM model with a moderate cutoff), the results are obscured by possible cutoff artifacts, in the "renormalized" version of the QM model they are spoiled by unphysical instabilities. We thus conclude that an approach beyond the present approximation is needed in order to resolve this problem.

VIII. CONCLUSIONS AND OUTLOOK

We have investigated inhomogeneous chiral-symmetry breaking phases at non-vanishing chemical potential and temperature within a two-flavor quark-meson model in the chiral limit. By comparing two different approximations of the thermodynamic potential the role of quantum fluctuations was addressed. We mainly focus on the effect of the quark Dirac sea, whose importance has recently been pointed out in [39] for homogeneous phases, but which had so far been neglected in QM-model studies of inhomogeneous phases [22]. In order to include these contributions to the thermodynamic potential, we introduced a consistent renormalization prescription. For the vacuum loops we employ the Pauli-Villars regularization and fix at a given value of the corresponding cutoff Λ the vacuum values of the constituent quark mass M, the pole mass of the sigma meson m_σ and the pion decay constant f_π. By increasing the cutoff Λ the results converge and already for $\Lambda \gtrsim 2$ GeV no numerical deviation is seen anymore both for homogeneous and inhomogeneous phases. In this way the model is effectively renormalized. For homogeneous phases the same asymptotic results are obtained if a sharp $O(3)$ cutoff regularization in momentum space is applied, which is, however, not suitable for inhomogeneous phases [8].

Within a Ginzburg-Landau analysis we have shown that for $m_\sigma = 2M$ the Lifshitz point of the inhomogeneous phase coincides with the tricritical point. Remarkably, this exactly corresponds to the NJL-model case where in the chiral limit m_σ always equals $2M$ [30] and the LP always coincides with the CP [8] (as long as no vector interactions are included [23]). In the QM model, however, m_σ can be varied independently from M, leading to scenarios where the LP and the CP are separated. These Ginzburg-Landau predictions are confirmed by our numerical results where we have considered one-dimensional modulations of the chiral order parameter. When the Dirac sea is included the inhomogeneous phase shrinks but in general does not disappear. The size of the inhomogeneous region is highly sensitive to the sigma mass and grows with increasing m_σ. As a consequence, for $m_\sigma > 2M$ it covers the entire first-order phase boundary between the homogeneous phases, including the CP, which thus disappears from the phase diagram. For $m_\sigma < 2M$, on the other hand, the inhomogeneous region covers at most the low-temperature part of the homogeneous first-order line or even vanishes completely.

Finally, we have explored the phase structure at high chemical potentials. For a moderate value of the cutoff, e.g., $\Lambda = 600$ MeV, an inhomogeneous "continent" appears, which is known from NJL-model investigations [24] but is not present in the sMFA. However, for large values of the cutoff, and in particular for the renormalized model, a general instability with respect to both, large amplitudes and large wave numbers of the chiral modulations are found. These numerical findings, in particular the unphysical instabilities, might be related to the used approximation. An improvement could be achieved, for example, via the functional renormalization group method, which has successfully been applied to the QM model for homogeneous phases [58] but not yet for inhomogeneous phases. In this way the influence of the mesonic quantum and thermal fluctuations on the thermodynamic potential can be analyzed in a systematic manner, in addition to the fermionic ones which have been studied in the present work. In general, it is known that the mesonic fluctuations are important not only in the vicinity of a phase transition but also to stabilize the system. On the other hand, inhomogeneous phases with one-dimensional modulations are expected to be unstable at finite temperature [59, 60], since the rigidity of the modulation is destroyed by thermal fluctuations. It would be interesting to see whether these effects can be studied straightforwardly by including mesonic fluctuations or whether additional degrees of freedom, in particular phonons, must be considered.

Acknowledgments

This work has been supported in part by the Helmholtz International Center for FAIR within the LOEWE program of the State of Hesse and by the Helmholtz Institute EMMI. B.-J.S. acknowledges support by the FWF Grant P24780-N27.

presentation transparent, the thermodynamic potential was plotted for the same fixed amplitude $\Delta = 75$ MeV for all curves shown in Fig. 12. For $\mu = 320$ and 485 MeV this is close to the values at the local minima for $\Lambda = 5$ GeV, which are given by $\Delta = 82$ and 74 MeV, respectively.

Appendix A: Dirac-sea contribution to the vacuum thermodynamic potential for small wave numbers

Inserting the density of states, Eq. (84), for $\Delta = M$ and $q < M$ into Eq. (90), one obtains

$$\begin{aligned}\Delta\Omega_{\mathrm{vac},q\bar{q}}(q) = -\frac{N_f N_c}{2\pi^2}\int_0^\infty dE\, E\,\Big\{&\theta(E-q-M)\sqrt{(E-q)^2-M^2}\,+\\ &\theta(E+q-M)\sqrt{(E+q)^2-M^2}\,-\\ &2\theta(E-M)\sqrt{E^2-M^2}\,\Big\}\,\sum_j c_j\sqrt{E^2+j\Lambda^2}\\ = -\frac{N_f N_c}{2\pi^2}\int_M^\infty dE\,\sqrt{E^2-M^2}\,\sum_j c_j\,\Big\{&(E+q)\sqrt{(E+q)^2+j\Lambda^2}\,+\\ &(E-q)\sqrt{(E-q)^2+j\Lambda^2}\,-\\ &2E\sqrt{E^2+j\Lambda^2}\,\Big\}\,,\end{aligned} \tag{A1}$$

where in the second step we have shifted the integration variable by $\pm q$ in the first two lines. Next, we Taylor-expand the integrand in q. This yields

$$\Delta\Omega_{\mathrm{vac},q\bar{q}}(q) = -\frac{N_f N_c}{2\pi^2}\int_M^\infty dE\, E\,\sqrt{E^2-M^2}\,\sum_j c_j\,\frac{2E^2+3j\Lambda^2}{(E^2+j\Lambda^2)^{3/2}}\,q^2\,+\,\mathcal{O}(q^4)\,. \tag{A2}$$

Substituting $p := \sqrt{E^2-M^2}$ and comparing the result with Eq. (41), one finds

$$\begin{aligned}\Delta\Omega_{\mathrm{vac},q\bar{q}}(q) &= -\frac{N_f N_c}{2\pi^2}\int_0^\infty dp\, p^2\,\sum_j c_j\,\frac{2p^2+2M^2+3j\Lambda^2}{(p^2+M^2+j\Lambda^2)^{3/2}}\,q^2\,+\,\mathcal{O}(q^4)\\ &= -M^2L_2(0)q^2 - \frac{N_f N_c}{2\pi^2}\int_0^\infty dp\, p^2\,\sum_j c_j\,\frac{2p^2+3M^2+3j\Lambda^2}{(p^2+M^2+j\Lambda^2)^{3/2}}\,q^2\,+\,\mathcal{O}(q^4)\,.\end{aligned} \tag{A3}$$

The remaining integral can be written as a total derivative

$$\Delta\Omega_{\mathrm{vac},q\bar{q}}(q) = -M^2L_2(0)q^2 - \frac{N_f N_c}{2\pi^2}\int_0^\infty dp\,\sum_j c_j\,\frac{d}{dp}\frac{p^3}{\sqrt{p^2+M^2+j\Lambda^2}}\,q^2\,+\,\mathcal{O}(q^4)\,, \tag{A4}$$

and, thus, vanishes in PV regularization. Hence, we are left with

$$\Delta\Omega_{\mathrm{vac},q\bar{q}}(q) = -M^2L_2(0)q^2\,+\,\mathcal{O}(q^4)\,, \tag{A5}$$

which is just Eq. (92).

[1] P. Braun-Munzinger and J. Wambach, Rev.Mod.Phys. **81**, 1031 (2009).
[2] K. Fukushima and T. Hatsuda, Rept.Prog.Phys. **74**, 014001 (2011).
[3] Y. Aoki, G. Endrodi, Z. Fodor, S. Katz, and K. Szabo, Nature **443**, 675 (2006).
[4] S. Borsanyi, G. Endrodi, Z. Fodor, S. D. Katz, S. Krieg, et al., PoS **LATTICE2011**, 201 (2011).
[5] C. Ratti, S. Borsanyi, G. Endrodi, Z. Fodor, S. D. Katz, et al., Nucl. Phys. **A904-905**, 869c (2013).
[6] A. Bazavov et al. (MILC Collaboration), PoS **LATTICE2012**, 071 (2012).
[7] B. Friman, C. Höhne, J. Knoll, S. Leupold, J. Randrup, et al., Lect.Notes Phys. **814**, 1 (2011).
[8] D. Nickel, Phys.Rev.Lett. **103**, 072301 (2009).
[9] P. Fulde and R. A. Ferrell, Phys.Rev. **135**, A550 (1964).
[10] A. Larkin and Y. Ovchinnikov, Zh.Eksp.Teor.Fiz. **47**, 1136 (1964).
[11] A. Overhauser, Phys.Rev. **128**, 1437 (1962).

[12] G. J. Conduit, A. G. Green, and B. D. Simons, Phys.Rev.Lett. **103**, 207201 (2009).
[13] M. G. Alford, J. A. Bowers, and K. Rajagopal, Phys.Rev. **D63**, 074016 (2001).
[14] R. Anglani, R. Casalbuoni, M. Ciminale, R. Gatto, N. Ippolito, et al., arXiv:1302.4264 [hep-ph].
[15] F. Dautry and E. Nyman, Nucl.Phys. **A319**, 323 (1979).
[16] A. S. Goldhaber and N. Manton, Phys.Lett. **B198**, 231 (1987).
[17] A. Heinz, F. Giacosa, and D. H. Rischke, arXiv:1312.3244 [nucl-th].
[18] W. Broniowski, A. Kotlorz, and M. Kutschera, Acta Phys.Polon. **B22**, 145 (1991).
[19] W. Broniowski and M. Kutschera, Phys.Lett. **B242**, 133 (1990).
[20] M. Sadzikowski and W. Broniowski, Phys.Lett. **B488**, 63 (2000).
[21] E. Nakano and T. Tatsumi, Phys.Rev. **D71**, 114006 (2005).
[22] D. Nickel, Phys.Rev. **D80**, 074025 (2009).
[23] S. Carignano, D. Nickel, and M. Buballa, Phys.Rev. **D82**, 054009 (2010).
[24] S. Carignano and M. Buballa, Acta Phys.Polon.Supp. **5**, 641 (2012).
[25] K. Fukushima, Phys.Rev. **D86**, 054002 (2012).
[26] S. Carignano and M. Buballa, Phys.Rev. **D86**, 074018 (2012).
[27] D. Müller, M. Buballa, and J. Wambach, Phys.Lett. **B727**, 240 (2013).
[28] T. Tatsumi, K. Nishiyama, and S. Karasawa, arXiv:1312.0307 [hep-ph].
[29] U. Vogl and W. Weise, Prog.Part.Nucl.Phys. **27**, 195 (1991).
[30] S. Klevansky, Rev.Mod.Phys. **64**, 649 (1992).
[31] T. Hatsuda and T. Kunihiro, Phys.Rept. **247**, 221 (1994).
[32] M. Buballa, Phys.Rept. **407**, 205 (2005).
[33] H. Abuki, D. Ishibashi, and K. Suzuki, Phys.Rev. **D85**, 074002 (2012).
[34] D. Deryagin, D. Y. Grigoriev, and V. Rubakov, Int.J.Mod.Phys. **A7**, 659 (1992).
[35] E. Shuster and D. Son, Nucl.Phys. **B573**, 434 (2000).
[36] T. Kojo, Y. Hidaka, L. McLerran, and R. D. Pisarski, Nucl.Phys. **A843**, 37 (2010).
[37] O. Scavenius, A. Mocsy, I. Mishustin, and D. Rischke, Phys.Rev. **C64**, 045202 (2001).
[38] B.-J. Schaefer and J. Wambach, Phys.Rev. **D75**, 085015 (2007).
[39] V. Skokov, B. Friman, E. Nakano, K. Redlich, and B.-J. Schaefer, Phys.Rev. **D82**, 034029 (2010).
[40] B.-J. Schaefer and M. Wagner, Phys.Rev. **D85**, 034027 (2012).
[41] J. O. Andersen, R. Khan, and L. T. Kyllingstad, arXiv:1102.2779 [hep-ph].
[42] U. S. Gupta and V. K. Tiwari, Phys.Rev. **D85**, 014010 (2012).
[43] H. Mao, J. Jin, and M. Huang, J.Phys. **G37**, 035001 (2010).
[44] U. S. Gupta and V. K. Tiwari, Phys.Rev. **D81**, 054019 (2010).
[45] B.-J. Schaefer, M. Wagner, and J. Wambach, Phys.Rev. **D81**, 074013 (2010).
[46] S. Chatterjee and K. A. Mohan, Phys.Rev. **D85**, 074018 (2012).
[47] M. D. Scadron, G. Rupp, and R. Delbourgo, Fortsch.Phys. **61**, 994 (2013).
[48] D. U. Jungnickel and C. Wetterich, Phys. Rev. **D53**, 5142 (1996).
[49] N. Strodthoff, B.-J. Schaefer, and L. von Smekal, Phys.Rev. **D85**, 074007 (2012).
[50] B.-J. Schaefer and J. Wambach, Nucl.Phys. **A757**, 479 (2005).
[51] G. Basar, G. V. Dunne, and M. Thies, Phys.Rev. **D79**, 105012 (2009).
[52] O. Schnetz, M. Thies, and K. Urlichs, Annals Phys. **314**, 425 (2004).
[53] J. Beringer et al. (Particle Data Group), Phys.Rev. **D86**, 010001 (2012).
[54] J. Pelaez, Phys.Rev.Lett. **92**, 102001 (2004).
[55] D. Parganlija, P. Kovacs, G. Wolf, F. Giacosa, and D. H. Rischke, Phys.Rev. **D87**, 014011 (2013).
[56] B.-J. Schaefer and M. Wagner, Phys.Rev. **D79**, 014018 (2009).
[57] S. R. Coleman and E. J. Weinberg, Phys.Rev. **D7**, 1888 (1973).
[58] B.-J. Schaefer and J. Wambach, Phys.Part.Nucl. **39**, 1025 (2008).
[59] G. Baym, B. Friman, and G. Grinstein, Nucl.Phys. **B210**, 193 (1982).
[60] L. Landau and E. Lifshitz, Statistical Physics (Addison-Wesley, Reading, MA, 1969).